Ultrasound in Med. & Biol., Vol. 40, No. 1, pp. 244–257, 2014

0301-5629/$ - see front matter

http://dx.doi.org/10.1016/j.ultrasmedbio.2013.08.015

● *Original Contribution*

3-D HIGH-FREQUENCY ULTRASOUND BACKSCATTER ANALYSIS OF HUMAN ARTICULAR CARTILAGE

Nils Männicke,* Martin Schöne,* Matthias Gottwald,† Felix Göbel,‡ Michael L. Oelze,§ and Kay Raum*‖

*Julius Wolff Institute and Berlin-Brandenburg School for Regenerative Therapies, Charité-Universitätsmedizin Berlin, Berlin, Germany; †Department of Surgery, Hospital Köln-Holweide, Cologne, Germany; ‡Department of Orthopaedics and Traumatology, Carl-von-Basedow-Klinikum, Merseburg, Germany; §Bioacoustics Research Laboratory, Department of Electrical and Computer Engineering, University of Illinois at Urbana-Champaign, Urbana, Illinois, USA; and ‖Department of Orthopedics, Martin Luther University of Halle-Wittenberg, Halle, Germany

(*Received* 19 *April* 2013; *revised* 13 *August* 2013; *in final form* 16 *August* 2013)

Abstract—High-frequency ultrasound is a promising method for non-invasive characterization of cartilage degeneration. Surface reflection and integrated spectral parameters are often used. In the work described here, human cartilage samples with varying degrees of degeneration were measured using a 40-MHz transducer. Backscatter signals originating from the superficial and transitional zones of cartilage were analyzed using amplitude, spectral and envelope statistical parameters and related to degenerative changes of the matrix given by the Mankin score. The results indicate an increased sensitivity of spectral slope and envelope statistical parameters to early matrix degeneration compared with conventional amplitude parameters. Furthermore, moderate correlations of chondrocyte number with backscatter amplitude and envelope statistics were observed, suggesting that at high frequencies, cells are one important scattering source in cartilage. An application of spectral and envelope statistical parameters to intra-articular ultrasound arthroscopy is conceivable and could improve the diagnostic potential of these examinations. Future studies are necessary to clarify the contributions of chondrocytes, extracellular matrix and collagen content to ultrasound backscatter to further improve the diagnostic potential of ultrasound for cartilage assessment. (E-mail: kay.raum@charite.de) **© 2014 World Federation for Ultrasound in Medicine & Biology.**

Key Words: **Backscatter, Cartilage, Degeneration, Envelope statistics, High-frequency ultrasound, Osteoarthritis, Quantitative ultrasound, Spectral slope, Ultrasound bio-microscopy, Ultrasound spectroscopy.**

INTRODUCTION

Osteoarthrosis (OA) is the most prevalent joint disease and results in considerable economic hardship and a decrease in quality-adjusted life years (Pinto et al. 2012). OA involves progressive degenerative changes in cartilage surface, matrix and subchondral bone. One of the first signs of OA is cartilage tissue softening, leading to cartilage fibrillation and disruption of the collagen network in later stages (Schöne et al. 2013). To date, none of the established non-invasive imaging modalities are able to assess these degenerative tissue alterations concurrently. Therefore, the gold standard is still histologic evaluation, for example, the Mankin (Buckwalter and Mankin 1998), Osteoarthritis Research Society International (Pritzker et al. 2006) and International Cartilage Repair Society II (Mainil-Varlet et al. 2010) scores. Non-invasive determination of different stages of degeneration is of high interest. In particular, the detection of the earliest signs of matrix degeneration, which are not associated with collagen destruction, could aid in the development of treatment strategies that aim to arrest the degeneration process (Brown et al. 2012; Yang et al. 2004).

In principle, high-frequency ultrasound is able to provide distinct information on the cartilage surface, cartilage matrix and subchondral bone boundary through temporal and inclination-controlled separation of the reflected and backscattered signals (Schöne et al. 2013). The use of ultrasound for the detection of early degenerative changes has been proposed in previous studies (Nieminen et al. 2009). The temporal variability and

Address correspondence to: Kay Raum, Julius Wolff Institut & Berlin-Brandenburg School for Regenerative Therapies, Charité-Universitätsmedizin Berlin, Augustenburger Platz 1, 13353 Berlin, Germany. E-mail: kay.raum@charite.de

intensity of signals reflected from the cartilage surface are related to cartilage surface roughness and stiffness, respectively, which are associated with collagen depletion (Nieminen et al. 2002; Wang et al. 2010), surface fibrillation (Saarakkala et al. 2004; Schöne et al. 2013) and biomechanical competence (Gelse et al. 2010) of the tissue. However, several researchers have noted that careful control of normal sound incidence is required for reliable estimation of reflection intensity and roughness parameters (Kaleva et al. 2009; Schöne and Raum 2011; Schöne et al. 2013). With increasing surface inclination, the fraction of specular reflection that is received by the transducer decreases, and the first detected signals become increasingly composed of sub-surface backscatter signals. Moreover, the intensity of the reflection from the interface between cartilage and subchondral bone has been observed to increase in OA samples, it has been suggested that this increase is due to a sclerosis-related increase in bone density (Jaffre et al. 2003; Laasanen et al. 2006; Saarakkala et al. 2006). As discussed by Saarakkala et al. (2011), the measured intensity from this interface is also subject to changes caused by alterations in sound attenuation in the cartilage matrix. Hence, *a priori* information on the acoustic properties of the matrix, that is, speed of sound and acoustic attenuation, is necessary to enhance the accuracy of parameters derived from the subchondral bone interface.

Only a few studies have investigated acoustic backscatter originating from the cartilage matrix for detection and characterization of cartilage degeneration, and so far, only integrated spectral amplitudes of the received signals have been considered, that is, apparent integrated backscatter (*AIB*). For example, Cherin et al. (1998) suggested that variations in *AIB* reflect changes in shape, size and/or density of scatterers in the cartilage matrix and could also be related to constitutional and structural changes in the extracellular cartilage matrix. However, until now, the origin of acoustic backscatter from cartilage tissue has not been fully identified. Experimentally, it has been found that *AIB* is not affected by depletion of proteoglycans (Pellaumail et al. 2002), but decreases with age in patellas of Wistar rats (Cherin et al. 2001) and after an acute impact injury in bovine bone (Viren et al. 2012). In contrast, a massive increase in *AIB* was observed in repair tissue as compared with intact hyaline cartilage (Gelse et al. 2010; Viren et al. 2010).

Much of ultrasound backscatter arises from sub-wavelength structures. In contrast to specular reflections, the spectrum of backscattered waves is usually not equivalent to that of incident waves. The spectrum of a backscattered signal received by an ultrasound probe from a scattering tissue is determined by distribution, geometry and acoustic impedance mismatch between scatterers and the surrounding medium. Outstanding work has been conducted in both theoretical formulations (Insana and Hall 1990; Lizzi et al. 1983) and experimental applications (Oelze and O'Brien 2006; Oelze et al. 2004) to use quantitative backscatter parameters, for example, the ultrasonic backscatter coefficient, to enhance the diagnostic power of clinical ultrasound scanners (Nam et al. 2012). However, for cartilage tissue, incorporation of spectral features more sophisticated than integrated intensity has not been achieved. One reason is that estimation of the backscatter coefficient requires locally homogeneous and uniform scattering properties in the direction of sound propagation, with axial dimensions on the order of several pulse lengths. The layered cartilage structure consisting of three thin layers, in which cells and collagen fibrils gradually change geometry, density and orientation (Fig. 1), leads not only to a pronounced dependence of acoustic backscatter on depth (Gelse et al. 2010), but also to gradual changes in bulk properties, for example, speed of sound and attenuation (Agemura et al. 1990).

To overcome these limitations, we applied 3-D high-frequency ultrasound in combination with depth-dependent spectral analysis using short time gates to the analysis of healthy and degenerated human cartilage samples. To separate specular surface reflections from components backscattered from cartilage matrix, we

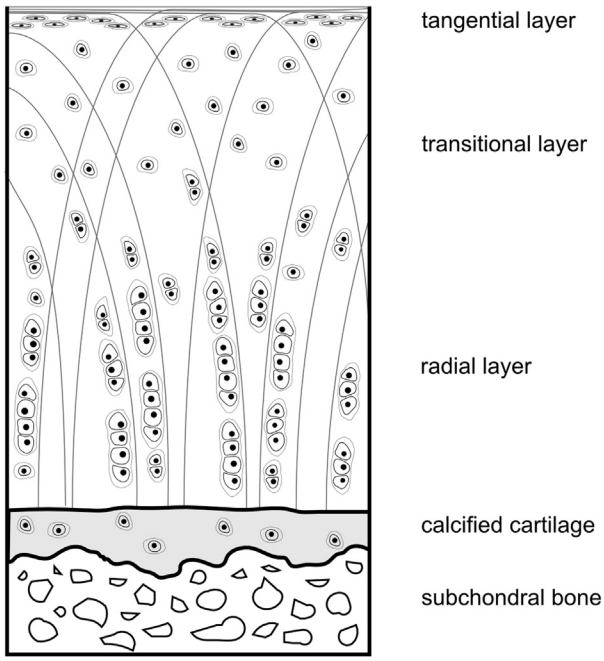

Fig. 1. Layered structure of healthy articular cartilage. The superficial zone is characterized by a large number of small disk-shaped chondrocytes. Fewer and more isotropic chondrocytes can be observed in the transitional zone. In the radial zone, chondrons contain multiple chondrocytes. Cell density is lowest and the cell size is large. Note the arch-like structure of collagen, with the fiber orientation parallel to the surface in the superficial zone and perpendicular to the surface in the radial zone.

applied distinct analyses in regions measured with normal and oblique incidence.

The aims of this study were: (i) to precisely separate signal contributions arising from specular reflections from sub-surface cartilage matrix backscatter; (ii) to analyze the diagnostic value of the frequency dependence of backscattered signals and the statistics of the envelope of backscattered signals; and (iii) to evaluate if and to what degree reflected and backscattered signals provide complementary information on specific signs of cartilage degeneration.

METHODS

Samples

This work was based on the same set of measurements used in a previous study and reported in detail therein (Schöne et al. 2013). Briefly, one to four punch biopsies (diameter = 8 mm) of degenerated cartilage were obtained from the femoral condyles of 19 patients, yielding 38 samples with variable degrees of degeneration. Biopsy specimens with highly degenerated cartilage (deep fissures or almost complete loss of cartilage, N = 2) were excluded from the study. Additionally, punch biopsies (N = 10) from the femoral joint were obtained within 24 h postmortem from four human cadavers with no degenerative joint disease. To ensure equal preparation conditions, all samples (N = 46) were immediately stored at –32°C. Before ultrasound measurements, the samples were thawed in phosphate-buffered saline at room temperature for 30 min, thereby ensuring that preparation procedures and storage times for all investigated biopsies were identical. Approval for the experiments was granted by the ethics committee of Martin-Luther-University Halle-Wittenberg and approved by a local institutional review board. Informed consent for the study was obtained from all patients.

Furthermore, a sample containing finely powdered graphite particles immersed in agar (Lakshmanan et al. 2012), which mimics variations in axial pressure amplitude in a scattering medium, was used as a reference material. The diameter and packing density of the particles were estimated from a cross section and were in the ranges 1.1 to 1.5 μm and 2376 to 3076 mm^{-2}, respectively.

Histology

After ultrasound measurements, histologic analysis was performed on demineralized and paraffin-embedded sections of the respective punch biopsies using routine histology processing and staining (safranin-O, hematoxylin and eosin) (Nieminen et al. 2002; Tunis et al. 2005). Serial transverse sections (5 μm thick) were cut through the central part of the biopsy. Cartilage degeneration was graded using the individual scoring categories (*i.e.,* cartilage surface, cells, extracellular matrix proteins and subchondral bone integrity) of the 14-point modified Mankin score (van der Sluijs et al. 1992). Of particular interest in this study were surface structure (referred to as Mankin I) and scoring of cellular abnormalities (referred to as Mankin II). Moreover, safranin-O matrix staining was performed on all samples. However, the quality and reproducibility of the safranin-O-stained sections were not sufficient to be included in the analysis. Two trained clinicians independently performed the scoring. They re-evaluated all scores that differed until they reached a consensus. Cells in one histologic section from each biopsy, in a 1-mm^2 square area directly below the cartilage surface, were counted manually. Custom-developed software was used in area selection and cell number density calculation.

Ultrasound bio-microscopy measurements

Cartilage samples were immersed at 25°C in phosphate-buffered saline and measured in C-scan mode (scan increment: 20 μm in x and y directions) using the custom scanning acoustic microscope SAM200Ex (Gelse et al. 2010; Leicht and Raum 2008; Schöne et al. 2013). The SAM is controlled by custom software (SAMEx, Q-BAM, Halle, Germany) and consists of a three-axis high-precision scanning stage, a 200-MHz pulser/receiver (Panametrics 5900 PR, Waltham, MA, USA) and a 500 MS/s A/D card (Gage CS8500, Gage Applied Technologies, Lachine, QC, Canada). A spherically focused 40-MHz lithium niobate transducer (f-number = 2.66, diameter = 3 mm, NIH Resource Center for Ultrasound Transducer Technology, Los Angeles, CA, USA) was used, providing lateral and axial resolutions of 120 and 50 μm, respectively. The measured center frequency at the focus was 37.5 MHz and the –6-dB range was 25–50 MHz, which corresponds to a fractional –6-dB bandwidth of 65%. The pulse length, defined as the –20-dB confocal pulse duration, was 60 ns. The focal distance was 9 mm, and the transducer-sample distance was adjusted so that the focal plane of the transducer was approximately 0.5 mm beneath the cartilage surface.

Data analysis

Offline data processing was performed with custom-designed toolboxes and functions written in C++ and MATLAB R2009b (The Mathworks, Natick, MA, USA).

Local surface position and inclination. For every scan point, the sample surfaces were approximated using a threshold method combined with spatial filtering, resulting in a map denoted by $d(x, y)$. On the basis of these surface positions, the local inclination $\theta_{\text{local}}(x, y)$ was estimated from the eigenvectors of the covariance matrix with a kernel size of 240 × 240 μm^2. $\theta_{\text{local}}(x, y)$ was fitted to a polynomial to obtain a smooth inclination map,

denoted $\theta_{global}(x, y)$. A detailed description of the procedure is given in Schöne et al. (2013). The speed of sound of the coupling medium used for the conversion from pulse-echo travel times to spatial distances was $c_0 = 1540$ m/s. In this study, two lateral regions of interest were selected based on restrictions on the global inclination. One region included waveforms from regions in which the global inclination was between 0° and 5° (hereafter called *normal incidence regions*), whereas regions with global inclination angles between 10° and 15° are referred to as *oblique incidence regions*.

Spectral analysis of backscatter. Backscatter power spectra $|S(f,x,y,z)|^2$ at the lateral position (x, y) and transducer gate distance z were estimated by calculating the squared magnitude of the fast Fourier transform of Hamming-windowed time signals with a duration of 2.5 pulse lengths (150 ns, corresponding to approximately 120 μm). In other studies, in which the dependence of ultrasound backscatter on frequency was used for tissue characterization, several pulse lengths were used for gating the signal. For example, 12 pulse lengths were chosen by Oelze and O'Brien (2006) to differentiate between carcinoma and sarcoma in a mouse mammary cancer model. In this study, a short gate length was necessary to accommodate the expected rapid change in tissue properties along the sound propagation direction. However, because the structure in each cartilage layer can be assumed to be relatively invariant in the lateral direction (*i.e.,* parallel to the cartilage surface), the spectra can be averaged in this direction, and therefore, statistical compensation becomes possible; that is, the variance of estimates can be reduced (Oelze and O'Brien 2004).

Reference spectrum. One calibration spectrum $\left|S_{ref}(f,z_0)\right|^2$ obtained from the planar reflection of a polymethylmethacrylate (PMMA) block at focus z_0 was used to compensate for the effects of system and transducer transfer functions. Many studies incorporate time-of-flight matched spectra from planar reflectors to additionally compensate for diffraction effects and the loss of pressure amplitude at defocused gate positions. However, for the chosen transducer, we have observed a considerable impact of phase interference artifacts, in the case of a planar reflection, on both amplitude (Schöne et al. 2013) and frequency dependence (see Appendix 2). Therefore, an amplitude correction for defocused positions was achieved by using the backscatter intensity from the agar-graphite phantom, and diffraction effects were neglected. This approach is feasible as long as the time gates remain within the focal region (–6 dB) of the transducer (Lizzi et al. 2003). The reference spectra of different axial positions can then be expressed as

$$S_{ref}(f,z) = \frac{S_{ref}(f,z_0)}{R_{PMMA}} \cdot \frac{I_{graphite}(z)}{I_{graphite}(z_0)}, \tag{1}$$

where $R_{PMMA} = 0.281$ is the reflection coefficient of PMMA, and $I_{graphite}(z)/I_{graphite}(z_0)$ denotes the normalized depth-dependent backscatter intensity from the graphite phantom within the –6-dB bandwidth of the transducer.

Backscatter amplitude. The *AIB* was introduced by Cherin et al. (1998) and quantifies the backscattered energy in the –6-dB bandwidth of the transducer from signals at different time gates. *AIB* is a function of tissue depth z_s relative to the cartilage surface $d(x, y)$:

$$AIB(z_s) = \frac{1}{N_{x,y}\cdot \Delta f} \sum_{x,y}^{Nx,y} \sum_{\Delta f} 10\cdot\log_{10}\left\langle \frac{|S(f,x,y,z)|^2}{\left|S_{ref}\ (f,z)\right|^2} \right\rangle \tag{2}$$

where

$$z = z_s + d(x,y). \tag{3}$$

The conversion from surface time delays to tissue depths was performed assuming a constant speed of sound of $c_1 = 1620$ m/s within the cartilage tissue (Agemura et al. 1990). $N_{x,y}$ is the number of averaged waveforms. Individual spectra were removed before averaging, if the average amplitude within the –6-dB bandwidth was less than 2 dB larger than a previously determined noise level. The noise level was calculated for each measurement from time gates before the surface time position of the sample, i.e., from regions where no scatterers were present. In these time gates, the average spectral amplitude within the –6-dB bandwidth of the transducer was determined.

Backscatter frequency dependence. Similar to the formulation of the *AIB* in eqn (2), difference spectra were calculated as a function of tissue depth. Spectra obtained from deep regions of the tissue are affected by acoustic attenuation and are susceptible to noise artifacts. In addition to the aforementioned noise exclusion at 2 dB for single spectra, within laterally averaged spectra, all frequency contributions below 4 dB of the noise level were removed. If less than 20% of the initial bandwidth remained, the entire spectrum was excluded (Fig. 2). After averaging and normalization, the difference spectra $W(f, z_s)$ were calculated:

$$W(f,z_s) = \left(\frac{1}{N_{x,y}} \sum_{x,y}^{N_{x,y}} 10\cdot\log_{10}\left\langle |S(f,x,y,z)|^2 \right\rangle\right) - 10\cdot\log_{10}\left\langle \left|S_{ref}\ (f,z_0)\right|^2 \right\rangle. \tag{4}$$

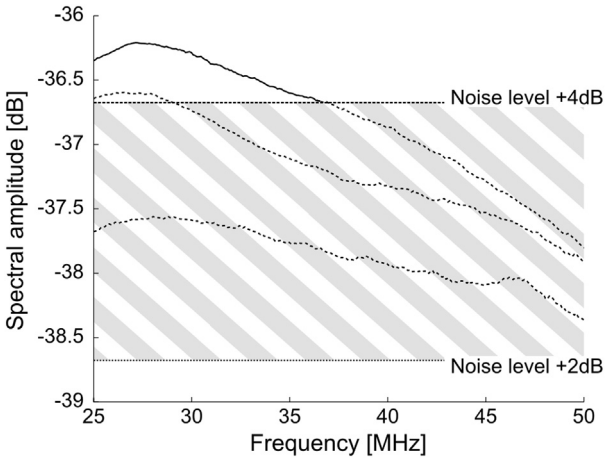

Fig. 2. Representative cases of noise exclusion after averaging. The dotted parts of the spectra were excluded because of insufficient amplitudes or insufficient remaining bandwidth. Solid lines indicate no exclusion.

Note that no amplitude correction was necessary, as only relative differences in the spectra were targeted. As proposed by Lizzi et al. (1997), linear regression analysis was applied within the bandwidth of the transducer, and the spectral slope was derived for each depth z_s. Because the *AIB* has been well established in assessing cartilage properties with ultrasound, we accordingly define this parameter as the apparent frequency dependence of backscatter (*AFB*).

Backscatter parameters in oblique incidence regions

As reported in our previous study (Schöne et al. 2013), no contributions of specular reflections occur beyond an inclination of 10° for the applied transducer, and the received signals from these locations are determined predominantly by the backscatter properties of sub-surface tissue. Therefore, the spectral slope $AFB_{\mathrm{surf}}^{10^\circ-15^\circ}$ and spectral amplitude $AIB_{\mathrm{surf}}^{10^\circ-15^\circ}$ were calculated from the detected surface ($z_s = 0$) (in oblique incidence regions) (Fig. 3a, c, e).

Depth-dependent backscatter parameters in normal incidence regions

In normal incidence regions, the aforementioned parameters were calculated as a function of depth using a sliding window technique (Gelse et al. 2010). The first window was centered at the detected surface position, and the maximum depth was set to 2.5 mm. A maximum overlap between adjacent gates was used (increment = 5 ns). For a strict differentiation between backscatter and the previously reported surface analysis, the surface reflection of the acquired voltage signal was gated out by adding the inverted signal multiplied by a Tukey window ($\alpha = 0.5$) at the center position of $z_s = 0$ with a gate length of 2.5 pulse lengths (Fig. 3b). Because the gate length was chosen to 2.5 pulse lengths, the center position of the first window that remains unaffected by this procedure is at a time delay of 2.5 pulse lengths, which corresponds to a tissue depth of 125 μm.

From each depth-dependent profile of *AIB* and *AFB* (Fig. 3d, f), the following parameters were extracted. $AIB_{\mathrm{max}}^{0^\circ-5^\circ}$ and $AFB_{\mathrm{max}}^{0^\circ-5^\circ}$ correspond to the maximum amplitude and spectral slope, respectively, of the backscatter from the superficial cartilage zone, which was approximated as the range from the cartilage surface to a depth of 300 μm. The decrease in parameter values with increasing depth ($AIB_{\mathrm{slope}}^{0^\circ-5^\circ}$ and $AFB_{\mathrm{slope}}^{0^\circ-5^\circ}$), as well as the extrapolation to the sample surface $z_s = 0$ ($AIB_{0}^{0^\circ-5^\circ}$ and $AFB_{0}^{0^\circ-5^\circ}$), were quantified using linear regression analysis. The most suitable ranges of the fits were determined automatically by calculating the correlation coefficient of every possible segment of the profile. Correlation coefficients were weighted by the length of the segment to avoid too short and, therefore, unrepresentative segments. The maximum starting depth of the linear section was set to 300 μm to consistently address the transitional cartilage layer and provide a meaningful extrapolation to the surface. $AIB_{\mathrm{slope}}^{0^\circ-5^\circ}$ and $AFB_{\mathrm{slope}}^{0^\circ-5^\circ}$ are given in dB/mm and dB/mm/MHz, respectively, and account for two-way propagation losses. Therefore, in a medium with a homogeneous distribution of scatterers, these slopes would be determined by the acoustic attenuation in the medium.

Texture parameters in normal incidence regions

The normal incidence regions were further analyzed with envelope statistics. Specifically, the homodyned K distribution was used to model the signal amplitude of the envelope at tissue depths between 200 and 600 μm. A previously published algorithm was used to provide parameters from the backscattered envelope data (Hruska and Oelze 2009). The algorithm used the signal-to-noise ratio, skewness and kurtosis calculated for fractional order moments from the backscattered envelope to estimate parameters based on the homodyned K distribution descriptive of the underlying scatterer organization. The estimation routine provided k and μ parameters from each data sample. The k parameter is the ratio of coherent to incoherent signal energy, and the μ parameter is related to the scatterer number density per resolution cell. Before parameter estimations, the depth-dependent amplitude of the envelope signal was normalized by the average decrease in depth-dependent envelope amplitude of all samples within the same tissue depth range at normal incidence regions. In accordance with the aforementioned parameters, the derived texture parameters are denoted $k^{0^\circ-5^\circ}$ and $\mu^{0^\circ-5^\circ}$.

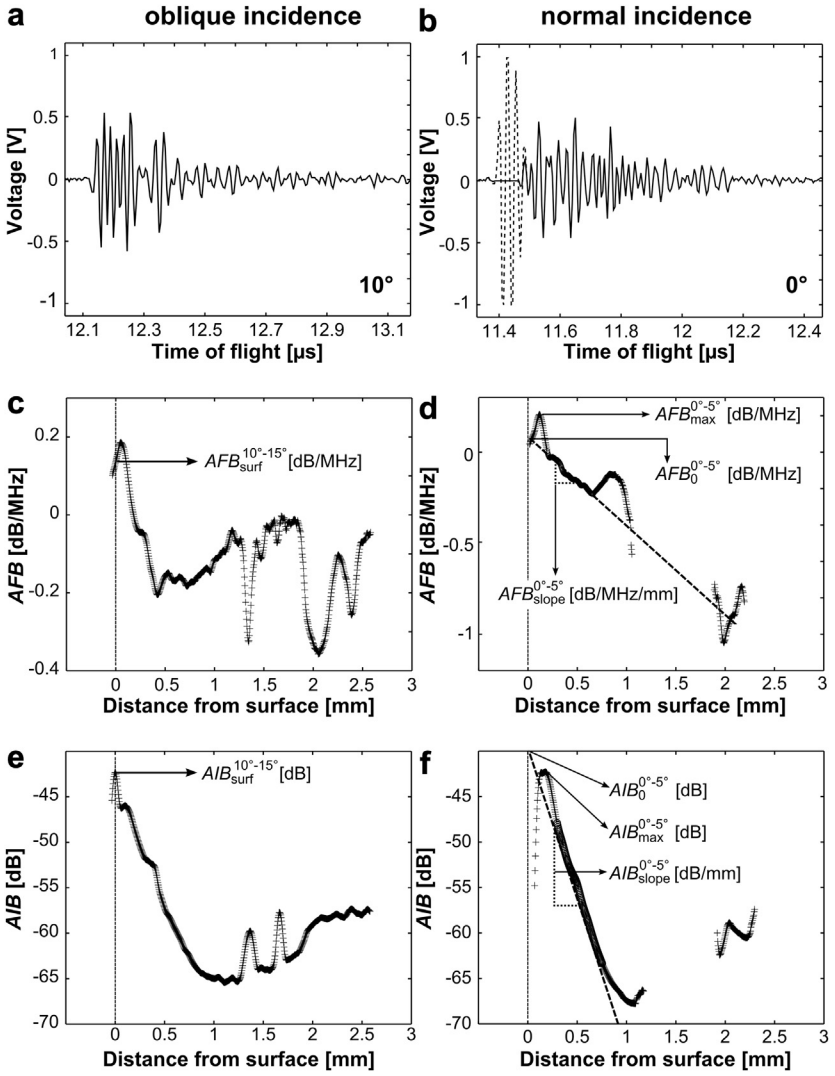

Fig. 3. Calculation of all eight parameters, divided into oblique incidence (a, c, e) and normal incidence (b, d, f). Representative pulse echoes are illustrated in (a) and (b). Note the surface exclusion indicated by the *dashed line* for normal incidence (b). In the oblique incidence case, frequency dependence (c) and the amplitude (e) were derived at the surface of the sample. In the normal incidence case, the maximum value as well as the slope and an extrapolation to the surface were derived for both frequency dependence (d) and amplitude (f) of backscatter. The most suitable range for linear regression analysis is indicated by *boldface data points*; linear models are represented by *dashed lines*.

Statistical analysis

One-way Kruskal-Wallis non-parametric analyses of variance were carried out using MATLAB R2009b to assess differences in backscatter parameters with respect to the cell Mankin score. Post hoc multiple comparison Tukey tests were used to identify differences among sub-groups. Correlations between ultrasonic and histologic parameters were analyzed using linear regression. Pearson's correlation was used to determine p-values, and R-square values were provided as measures for the goodness of fit. All results were considered significant at $p < 0.05$.

RESULTS

Histologic and acoustic appearance of healthy and degenerated cartilage

Mankin scores of the 46 biopsies covered a broad range of cartilage degeneration (Mankin I: 0 [$n = 8$, $D = 4$], 1 [$n = 8$, $D = 7$], 2 [$n = 11$, $D = 9$], 3 [$n = 13$, $D = 11$], 4 [$n = 6$, $D = 2$]; Mankin II: 0 [$n = 5$, $D = 4$], 1 [$n = 16$, $D = 11$], 2 [$n = 23$, $D = 16$], 3 [$n = 2$, $D = 2$], where n is number of biopsies and D is number of donors). The intra-donor average standard deviation was 0.45 for both Mankin I and

Mankin II. Two-dimensional cell density ranged between 48 and 325 mm^{-2} (mean ± standard deviation: 155 ± 62 mm^{-2}).

Not all acoustic parameters could be computed in all samples. In four samples, the oblique regions were not large enough to calculate $AFB_{surf}^{10°-15°}$ and $AFB_{surf}^{10°-15°}$. In seven samples, the range of linear decrease in $AFB(z_s)$ was too small (<300 μm) to fit a linear model to the data and to compute $AFB_{slope}^{0°-5°}$ and $AFB_{0}^{0°-5°}$. The maximum peak values $AFB_{max}^{0°-5°}$, all *AIB* parameters at normal incidence and both envelope statistical parameters could be calculated for all samples.

Depth-dependent backscatter and spectral parameters are illustrated in combination with histologic cross sections in Figure 4 for a healthy cartilage sample and a degenerated cartilage sample. The degenerative changes of the cartilage surface are manifested as both a lower reflection intensity and increased roughness of the surface. In the cross-sectional image, the backscatter from the matrix in the degenerated sample appears to be less homogeneous than that in the healthy sample. For example, on the left-hand side, the surface- and depth-dependent backscatter of the degenerated sample are similar to those observed in the healthy cartilage sample, whereas on the right-hand side, the sub-surface backscatter in the degenerated cartilage was much lower. In Figure 4g, the depth-dependent spectral slope profile of the healthy sample features a sub-surface peak, a linear decrease for approximately 500 μm and an apparent change in slope with another peak just before *AIB* reaches a minimum at a depth of approximately 1 mm. In contrast, in the degenerated sample, there is no sub-surface peak, and the linear slope of *AFB* is less steep (Fig. 4h); similar to the healthy sample, a change in slope can be observed below 0.6 mm. This change in slope coincided with a gradual change in chondrocyte appearance and cell number density, as observed in the histologic cross sections (Fig. 4i, j). On the histologic slide of the healthy sample, the cells of the different layers appear normal, and hyper-cellularity or clusters are not observed (Fig. 4i). However, in the degenerated cartilage sample, the layered architecture is less apparent and a large number of cell clusters are observed (Fig. 4j).

Quantitative analysis

Statistical evaluations were carried out for the described parameters with respect to Mankin I, Mankin II and cumulative scores. For comparison, the previously assessed surface parameters (median and 50% quantile length of the integrated reflection coefficient [*IRC* and *ΔIRC*, respectively]), as well as the ultrasonic roughness index [*URI*] (Schöne et al. 2013), were also included in the analysis (Table 1). All surface parameters provided statistically significant differences with respect to Mankin II and, with higher χ^2 values, to Mankin I. Higher significance levels were observed for *URI* ($p < 0.001$) than for *IRC* and *ΔIRC*. Mankin II had no significant effect on the variance of all *AIB* parameters, and only $AIB_{max}^{0°-5°}$ was statistically significantly different with respect to Mankin I. In contrast, Mankin II had significant effects on all four *AFB* parameters. Except for $AFB_{slope}^{0°-5°}$, all parameters were statistically significantly different with respect to Mankin I. With respect to the χ^2 values obtained, Mankin I had a more significant effect on all parameters than did Mankin II; however, only a small difference in significance levels between Mankin scores was observed for μ and *AFB* parameters at normal incidence. The highest significance levels and χ^2 values of all investigated parameters, with respect to all Mankin scores investigated, were obtained for $AFB_{max}^{0°-5°}$. As seen in Figure 5, this parameter has highly positive values for healthy cartilage, but significantly lower values for samples that exhibit degenerative signs of either surface or matrix properties.

Cross-correlations between all discrete parameters obtained were calculated to investigate whether the proposed parameters provide complementary information (Table 2). The surface parameters were moderately correlated. Furthermore, *URI* was moderately correlated with the frequency-dependent backscatter parameters $AFB_{surf}^{10°-15°}$ and $AFB_{max}^{0°-5°}$, and the *IRC* values were moderately correlated with amplitude parameters $AIB_{max}^{0°-5°}$ and $AIB_{0}^{0°-5°}$. Depth-dependent amplitude and frequency-dependent parameters were not correlated. Except for $AIB_{0}^{0°-5°}$ and $AIB_{max}^{0°-5°}$, which were highly correlated, correlations between all other parameters were low or moderate. Cell density was moderately correlated with $AIB_{0}^{0°-5°}$ and $AIB_{max}^{0°-5°}$ and weakly correlated with $\mu^{0°-5°}$.

Figure 6 summarizes the relationship between cell density and $AIB_{max}^{0°-5°}$. Linear regression revealed a positive correlation between the two parameters. Cell density with respect to Mankin II increased slightly, but not significantly, from Mankin II score 0 to score 1 and decreased at higher scores (Fig. 6b). The transition from hyper-cellularity (Mankin II = 1) to hypo-cellularity (Mankin II = 3) was associated with a significant decrease in cell density (Fig. 6b). A similar trend, but not statistically significantly different, was observed for $AIB_{max}^{0°-5°}$ (Fig. 6c).

Statistically significant differences were also observed for the envelope statistical parameter $\mu^{0°-5°}$, that is, the scatterer number density per resolution cell, with respect to Mankin II (Fig. 7). In contrast to the cell number densities assessed by histology, a significant difference was observed between Mankin II scores 0 and 2, corresponding to healthy tissue and chondrocyte

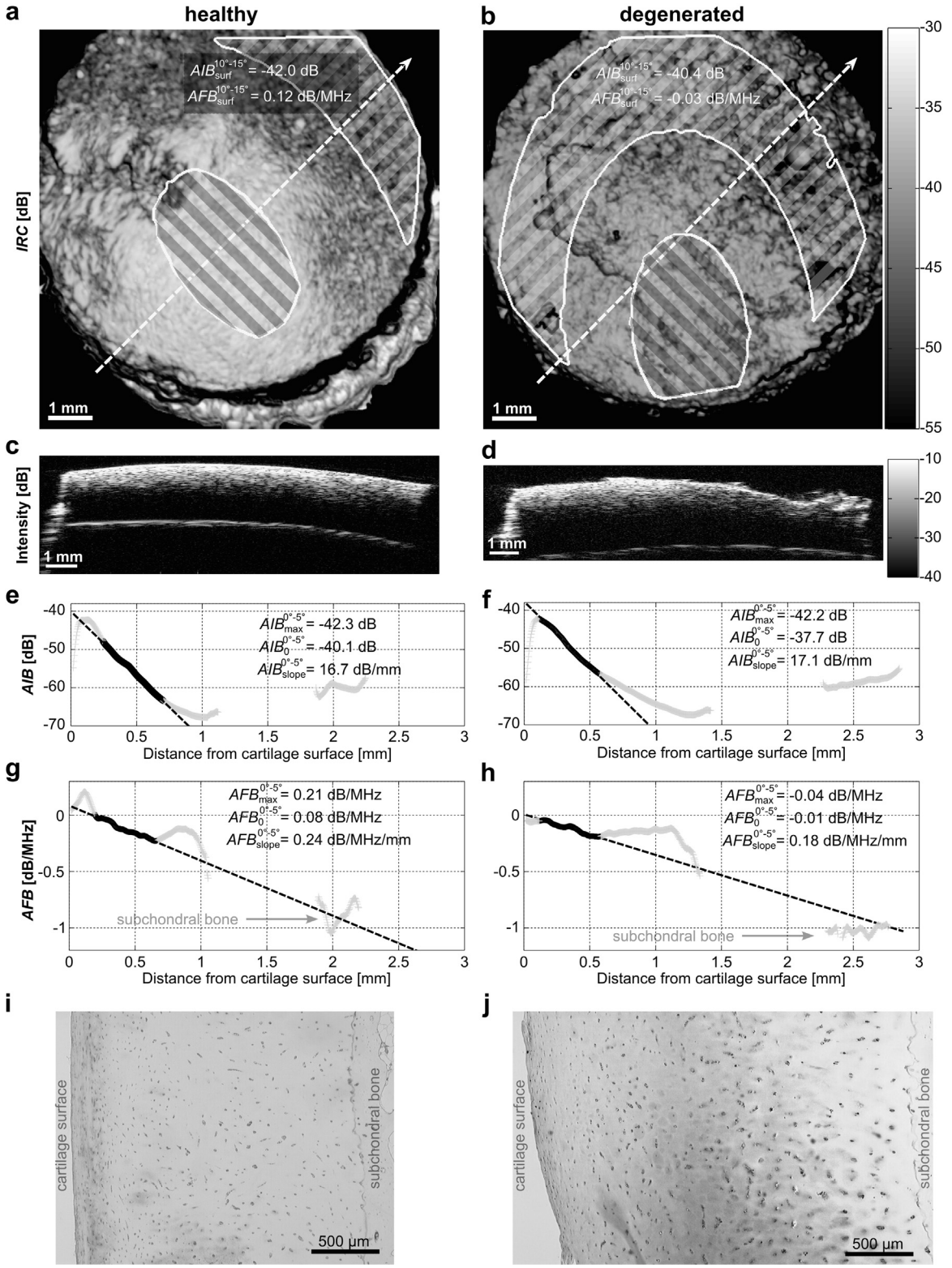

Fig. 4. Images of samples of healthy (Mankin I = 0, Mankin II = 0) and degenerated (Mankin I = 2, Mankin II = 2) cartilage. (a, b) Surface reflection maps as described in Schöne et al. (2013) on which locations of regions of low and high inclination in dark and bright hachures, respectively, are superimposed. (c, d) Positions of cross-sectional B-mode images (c, d) are indicated by *dashed arrows*. (g–j) Depth-dependent profiles of *AIB* (g, h) and *AFB* (i, j). The intercept with the *y*-axis corresponds to cartilage surface. (k, l) Corresponding histologic cross section.

Table 1. χ^2-values and significant score differences of the ultrasound parameters with respect to Mankin I, Mankin II and the cumulative Mankin scores. In contrast to amplitude based parameters, most spectral slope and envelope statistics parameters are statistically significantly different with respect to Mankin I and Mankin II*

	Mankin I	Mankin II	Cumulative Mankin
Surface parameters			
IRC	**16.83** (0 > 3,4)	**8.85** (0 > 3)	n.s.
ΔIRC	**17.94** (0 < 3,4)	**7.81** (0 < 2)	**18.17** (0 < 6)
URI	**19.59** (0 < 2,3)	**13.79** (0 < 1,2,3)	**17.01** (0 < 4,5)
Backscatter parameters at normal inclination			
$AIB_{max}^{0^\circ-5^\circ}$	**15.15** (0,1 > 4)	n.s.	**16.4** (2 > 6)
$AIB_{0}^{0^\circ-5^\circ}$	n.s.	n.s.	n.s.
$AIB_{slope}^{0^\circ-5^\circ}$	n.s.	n.s.	n.s.
$AFB_{max}^{0^\circ-5^\circ}$	**20.08** (0 > 1,2,3,4)	**14.44** (0 > 1,2)	**19.91** (0 > 3,4,6)
$AFB_{0}^{0^\circ-5^\circ}$	**13.61** (0 > 2,3)	**12.27** (0 > 1,2)	**14.87** (0 > 3,5)
$AFB_{slope}^{0^\circ-5^\circ}$	n.s.	**9.65** (0 > 1,2)	n.s.
Backscatter parameters at high inclination			
$AIB_{surf}^{10^\circ-15^\circ}$	n.s.	n.s.	n.s.
$AFB_{surf}^{10^\circ-5^\circ}$	**16.37** (0 > 2,3)	**8.47** (0 > 2)	n.s.
Envelope statistic parameters			
$\mu^{0^\circ-5^\circ}$	**13.99** (0 > 3,4)	**10.36** (0 > 2,3)	**15.0** (0 > 6)
$k^{0^\circ-5^\circ}$	n.s.	n.s.	n.s.

n.s. = not significant
* Values are /χ^2 (bold numbers) and group differences (in brackets).

clustering, respectively. No significant differences were observed for $k^{0^\circ-5^\circ}$.

DISCUSSION

In the present study, high-frequency ultrasound backscatter signals originating from the matrix of human articular cartilage were investigated and related to spontaneous degenerative changes in the course of osteoarthritis. For the first time, in addition to amplitude parameters, spectral parameters and envelope statistics were incorporated and, contrary to conventional approaches, strictly separated to analyze their diagnostic value. Our results suggest that spectral and envelope statistical parameters are sensitive to osteoarthritic changes of the cartilage matrix and out-perform purely amplitude-based parameters.

In a first approach, backscatter amplitude and frequency dependence were calculated at the tissue surface from highly inclined regions. As discussed in a previous work (Schöne et al. 2013), these received signals should be determined by acoustic and structural properties of superficial scatterers in the cartilage matrix. The present results confirm this hypothesis and reveal a significant relationship between frequency dependence of backscatter and degenerative changes in the matrix.

In a second step, the region of interest was changed to almost planar areas (*i.e.,* the same regions that were used to estimate surface parameters) so that the depth-dependent acoustic parameters can be linked to an idealized cross-sectional representation of collagen and chondrocytes within the different cartilage layers. It can be assumed that close to the surface, acoustic waves pass through a small tissue layer, in which the collagen fibers are aligned

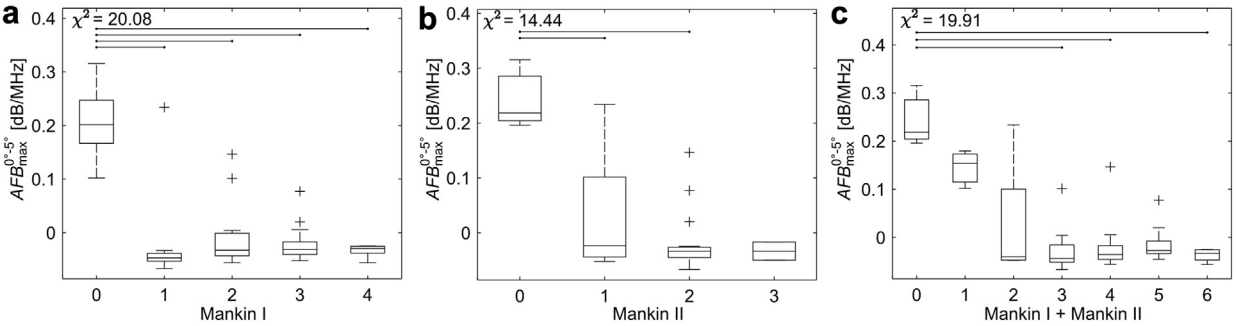

Fig. 5. Box plots of sub-surface peak $AFB_{max}^{0^\circ-5^\circ}$ with respect to Mankin I (a), Mankin II (b) and cumulative Mankin (c) scores. Statistically significant differences between the groups are indicated by the *horizontal lines* at the top.

Table 2. Correlation coefficients, R^2, between all ultrasound parameters and cell density

	IRC	*ΔIRC*	*URI*	$AIB_{max}^{0^\circ-5^\circ}$	$AIB_{0}^{0^\circ-5^\circ}$	$AIB_{slope}^{0^\circ-5^\circ}$	$AFB_{max}^{0^\circ-5^\circ}$	$AFB_{0}^{0^\circ-5^\circ}$	$AFB_{slope}^{0^\circ-5^\circ}$	$AIB_{surf}^{10^\circ-15^\circ}$	$AFB_{surf}^{10^\circ-15^\circ}$	$\mu^{0^\circ-5^\circ}$	$k^{0^\circ-5^\circ}$	Cell density
IRC	1.00	0.56	0.68	0.59	0.48	0.24	0.37	0.31	0.21	0.46	0.38	0.19	n.s.	0.18
ΔIRC		1.00	0.44	0.32	0.31	0.38	0.42	0.22	0.11	0.32	0.41	0.25	n.s.	n.s.
URI			1.00	0.26	0.32	0.28	0.53	0.33	0.23	0.17	0.48	0.19	n.s.	n.s.
$AIB_{max}^{0^\circ-5^\circ}$				1.00	0.80	0.25	0.08	n.s.	n.s.	0.45	0.16	0.27	n.s.	0.43
$AIB_{0}^{0^\circ-5^\circ}$					1.00	0.43	0.10	0.11	0.09	0.28	0.13	0.23	0.10	0.39
$AIB_{slope}^{0^\circ-5^\circ}$						1.00	n.s.	n.s.	0.09	0.13	0.20	n.s.	n.s.	n.s.
$AFB_{max}^{0^\circ-5^\circ}$							1.00	0.48	0.15	n.s.	0.53	0.19	n.s.	n.s.
$AFB_{0}^{0^\circ-5^\circ}$								1.00	0.68	0.12	0.27	0.12	n.s.	n.s.
$AFB_{slope}^{0^\circ-5^\circ}$									1.00	0.11	n.s.	n.s.	n.s.	n.s.
$AIB_{surf}^{10^\circ-15^\circ}$										1.00	0.11	n.s.	n.s.	0.17
$AFB_{surf}^{10^\circ-15^\circ}$											1.00	n.s.	n.s.	n.s.
$\mu^{0^\circ-5^\circ}$												1.00	n.s.	0.19
$k^{0^\circ-5^\circ}$													1.00	n.s.
Cell density														1.00

n.s. = not significant

parallel to the surface and the chondrocytes are minimal in cross section. In healthy cartilage samples, this zone had highly positive spectral slope values. The related parameter AFB_{max} exhibited the most significant variation with respect to cartilage matrix degeneration because of its ability to differentiate between Mankin II score 0 and Mankin II scores 1 and 2. According to scattering theory, a large positive slope of received backscatter spectra can be attributed to structures with dimensions much smaller than the wavelength ($ka << 1$). Such structures could be associated with the collagen network of the superficial zone and/or the large number of small chondrocytes in this tissue layer. One of the earliest signs of OA is disruption of superficial collagen (Buckwalter and Mankin 1998), which could explain the diminishment of this peak. On the other hand, the moderate correlation between cell

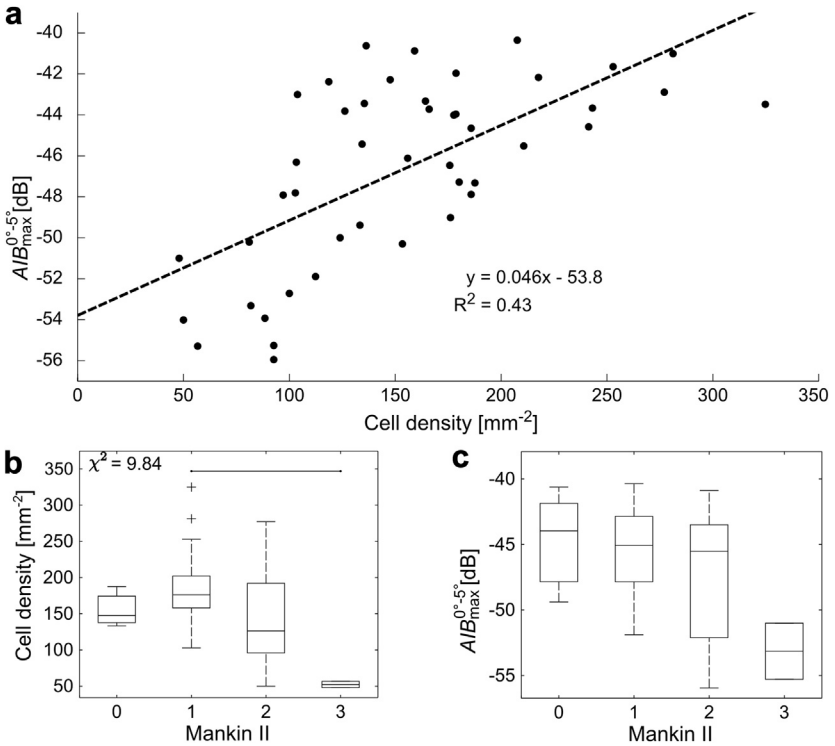

Fig. 6. Scatter plot of cell density versus $AIB_{max}^{0^\circ-5^\circ}$ in conjunction with a linear regression curve (a). The corresponding coefficients, as well as the goodness of fit, are included. Box plots of cell density (b) and $AIB_{max}^{0^\circ-5^\circ}$ (c) with respect to Mankin II score, respectively. The χ^2 value is provided if the Kruskal-Wallis test yielded statistical significance.

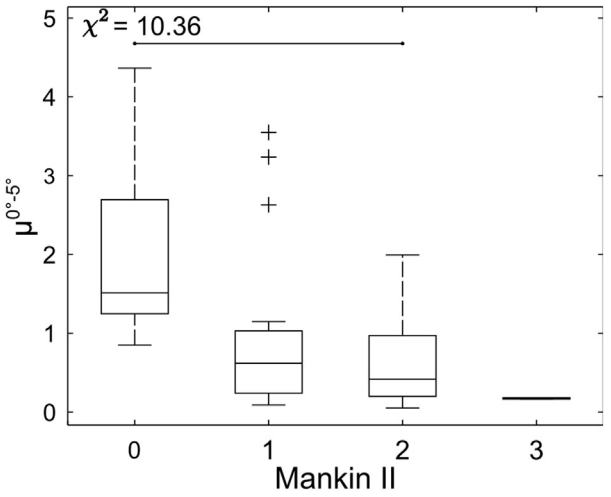

Fig. 7. Box plot of the scatterer number density per resolution cell $\mu^{0°-5°}$ with respect to Mankin II score.

number and scattering amplitude suggests chondrocytes are an important scattering source. Therefore, future studies should focus on elucidation of the relative contributions of acoustic backscatter from cells and collagen matrix, as this could serve as an important biomarker for early degenerative signs at the cellular level that are not associated with destruction of the collagen network.

From linear regression of the depth-dependent *AFB*, the slope with respect to tissue depth and the spectral slope at the surface were estimated. In a homogeneous medium with randomly distributed scatterers, these parameters carry important information. Namely, the depth-dependent slope relates to the frequency-dependent acoustic attenuation of the medium, and the extrapolated surface spectral slope is not affected by attenuation and can be used to estimate the size and shape of the scatterers. However, cartilage has a layered structure, and tissue properties must be assumed to differ between layers. Therefore, acoustic attenuation could not be derived from the backscattered signals in cartilage tissue. However, we observed regions with linear slopes in healthy cartilage tissue, and values derived from these regions were in agreement with attenuation values reported by others. For example, Nieminen et al. (2004) observed slightly higher values (0.40 ± 0.14 dB/mm/MHz) in healthy bovine tissue and decreased values in degenerated samples. In this study, numerous estimates of AFB_{slope} in degenerated samples were negative. However, it should be noted that in contrast to previous studies, in which attenuation was measured in transmission through all cartilage layers, AFB_{slope} was determined from backscattered signals from the transitional tissue zone only. Depth-dependent backscatter changes, for example, caused by the presence of large chondrocyte clusters in degenerated samples or superficial matrix fibrillation within this region, lead to maximum backscatter amplitude below the surface. Therefore, AFB_{slope} is not necessarily a surrogate for acoustic attenuation, particularly in degenerated tissue.

A reduction in the extrapolated spectral slope values AFB_0 was observed for degenerated cartilage samples. A potential explanation is a clustering of chondrocytes and increase in size of chondrons during progression of OA (Poole 1997), which can be hypothesized to cause a decrease in AFB_0 if the scatterer sources are sufficiently smaller than the wavelength. However, because of the negative estimations of AFB_{slope}, particularly in degenerated samples, some values of AFB_0 are under-estimated and also do not relate directly to the structural or elastic properties of the cartilage matrix. Furthermore, a distinct deviation from the linear depth-dependent decrease was observed for *AFB* in healthy samples at tissue depths between 0.5 and 1.0 mm (Fig. 3d). This depth corresponds to the transitional zone, in which the chondrocytes gradually increase in size and change their shape and arrangement to form spherical cell clusters (chondrons). Moreover, collagen content and fibril orientation, as well as the resulting elastic bulk properties, are subject to change in this region (Agemura et al. 1990; Leicht and Raum 2008). The presence and location of this feature in the *AFB* profile may therefore help to identify the zonal organization of the tissue.

Complementary to the frequency dependence of acquired spectra, the integrated spectral amplitude *AIB* has been addressed in this study. Despite a modification of the reference spectrum, *AIB* was calculated in a manner similar to that described in a previous study (Gelse et al. 2010). Compared with spectral parameters, *AIB* parameters are easier to derive, but exhibit weaker variations with respect to degenerative changes classified by the Mankin score. However, AIB_{max} and AIB_0 were moderately correlated with cell number, which explains the sensitivity to hyper-cellularity (Mankin II grade 1) and hypo-cellularity (Mankin II grade 3). Interestingly, the depth-dependent reduction in *AIB* (AIB_{slope}) did not provide statistically significant variations with respect to the evaluated Mankin scores, but has been found to be a highly predictive parameter for cartilage repair tissue (Gelse et al. 2010). The latter has been attributed to the different packing densities of collagen in hyaline and repair cartilage. The envelope statistics revealed significantly lower μ values for Mankin II grade 2 compared with healthy controls. In contrast, cell number density assessed by histology differed between grades 1 and 3. The reason for this discrepancy is that the cells were counted individually (regardless of cell clustering) in the histology analysis, whereas envelope statistics do not distinguish between an individual cell and a chondron containing two or

more cells. Therefore, the combination of several time-domain envelope and spectral parameters may enable identification of chondrocyte clustering.

Statistically significant differences were observed predominantly between the healthy group (Mankin I and II score 0) and all groups with Mankin scores > 0. This observation can be attributed to both a lack of sensitivity of the experimental methods and a lack of statistical power. The histologic scores were assessed from 2-D slides and were compared with ultrasound readings obtained from 3-D volumes. Therefore, the region evaluated by histology was only a sub-region of that evaluated by ultrasound. Spatially, local changes in tissue properties are likely, particularly in the higher stages of degeneration, which may have affected histologic and ultrasound readings to a different extent. As a result, the histologic scores cannot be expected to be fully comparable to the ultrasound parameters, and the limited number of samples evaluated in this study presumably prevented statistically significant differences among the groups, especially with respect to Mankin II grade 3 ($N = 2$). Taking this into consideration, a combination of several ultrasound parameters may enable better discrimination between early and moderate stages of degeneration.

Miniaturized intra-articular ultrasound devices have been found to be powerful arthroscopic tools that enable quantification of surface roughness, reflection intensity and subchondral bone parameters. This allows for objective and highly reproducible assessment of local cartilage degeneration (Kaleva et al. 2011; Liukkonen et al. 2013; Viren et al. 2011). Because the proposed intra-articular ultrasound devices operate at the same frequency used in this work, an extension toward *AFB* and envelope statistical parameters appears straightforward. However, future work should elaborate on the robustness of the proposed parameters, that is, the influence of local inclination, the applicability to intra-articular ultrasound devices and ideal dimensions of the region of interest. Furthermore, investigations are necessary to unravel specific links between spectral parameters and cellular and extracellular tissue structures. Although the spectral parameters investigated in this study proved to be sensitive to different OA-related tissue alterations, it is believed the introduction of more sophisticated data analysis, such as diffraction correction and the application of form factor models, would further improve the sensitivity and specificity of non-invasive assessment of cartilage quality using high-frequency ultrasound.

CONCLUSIONS

It has been found for the first time that envelope statistics and depth-dependent spectral slope parameters are sensitive to the early stages of extracellular matrix degeneration and outperform conventionally used amplitude-based parameters. An application to intra-articular ultrasound arthroscopies could improve the diagnostic potential of these examinations.

Acknowledgments—This work was supported by the German Research Council (DFG Grant Ra1380/6) and Deutsche Arthrose-Hilfe e.V. N.M. receives a DFG stipend through the Berlin-Brandenburg School for Regenerative Therapies GSC 203. The authors acknowledge Salma M. Thalji for assistance in the preparation of the article.

REFERENCES

Agemura DH, O'Brien WD, Olerud JE, Chun LE, Eyre DE. Ultrasonic propagation properties of articular cartilage at 100 MHz. J Acoust Soc Am 1990;87:1786–1791.

Brown CP, Oloyede A, Crawford RW, Thomas GER, Price AJ, Gill HS. Acoustic, mechanical and near-infrared profiling of osteoarthritic progression in bovine joints. Phys Med Biol 2012;57:547–559.

Buckwalter JA, Mankin HJ. Articular cartilage: Degeneration and osteoarthritis, repair, regeneration, and transplantation. Instr Course Lect 1998;47:487–504.

Cherin E, Saied A, Laugier P, Netter P, Berger G. Evaluation of acoustical parameter sensitivity to age-related and osteoarthritic changes in articular cartilage using 50-MHz ultrasound. Ultrasound Med Biol 1998;24:341–354.

Cherin E, Saied A, Pellaumail B, Loeuille D, Laugier P, Gillet P, Netter P, Berger G. Assessment of rat articular cartilage maturation using 50-MHz quantitative ultrasonography. Osteoarthritis Cartilage 2001;9:178–186.

Gelse K, Olk A, Eichhorn S, Swoboda B, Schöne M, Raum K. Quantitative ultrasound biomicroscopy for the analysis of healthy and repair cartilage tissue. Eur Cell Mater 2010;19:58–71.

Hruska DP, Oelze ML. Improved parameter estimates based on the homodyned K distribution. IEEE Trans Ultrason Ferroelectr Freq Control 2009;56:2471–2481.

Insana MF, Hall TJ. Parametric ultrasound imaging from backscatter coefficient measurements: Image formation and interpretation. Ultrason Imaging 1990;12:245–267.

Jaffre B, Watrin A, Loeuille D, Gillet P, Netter P, Laugier P, Saied A. Effects of antiinflammatory drugs on arthritic cartilage: A high-frequency quantitative ultrasound study in rats. Arthritis Rheum 2003;48:1594–1601.

Kaleva E, Saarakkala S, Jurvelin JS, Viren T, Toyras J. Effects of ultrasound beam angle and surface roughness on the quantitative ultrasound parameters of articular cartilage. Ultrasound Med Biol 2009;35:1344–1351.

Kaleva E, Viren T, Saarakkala S, Sahlman J, Sirola J, Puhakka J, Paatela T, Kröger H, Kiviranta I, Jurvelin JS, Toyras J. Arthroscopic ultrasound assessment of articular cartilage in the human knee joint. Cartilage 2011;2:246–253.

Laasanen MS, Toyras J, Vasara A, Saarakkala S, Hyttinen MM, Kiviranta I, Jurvelin JS. Quantitative ultrasound imaging of spontaneous repair of porcine cartilage. Osteoarthritis Cartilage 2006;14:258–263.

Lakshmanan S, Koch T, Brand S, Männicke N, Wicke M, Mörlein D, Raum K. Prediction of the intramuscular fat content in loin muscle of pig carcasses by quantitative time-resolved ultrasound. Meat Sci 2012;90:216–225.

Leicht S, Raum K. Acoustic impedance changes in cartilage and subchondral bone due to primary arthrosis. Ultrasonics 2008;48:613–620.

Liukkonen J, Hirvasniemi J, Joukainen A, Penttila P, Viren T, Saarakkala S, Kroger H, Jurvelin JS, Toyras J. Arthroscopic ultrasound technique for simultaneous quantitative assessment of articular cartilage and subchondral bone: An in vitro and in vivo feasibility study. Ultrasound Med Biol 2013;39:1460–1468.

Lizzi FL, Astor M, Liu T, Deng C, Coleman DJ, Silverman RH. Ultrasonic spectrum analysis for tissue assays and therapy evaluation. Int J Imaging Syst Technol 1997;8:3–10.
Lizzi FL, Feleppa EJ, Kaisar Alam S, Deng CX. Ultrasonic spectrum analysis for tissue evaluation. Pattern Recognition Lett 2003;24:637–658.
Lizzi FL, Greenebaum M, Feleppa EJ, Elbaum M, Coleman DJ. Theoretical framework for spectrum analysis in ultrasonic tissue characterization. J Acoust Soc Am 1983;73:1366–1373.
Mainil-Varlet P, Van DB, Nesic D, Knutsen G, Kandel R, Roberts S. A new histology scoring system for the assessment of the quality of human cartilage repair: ICRS II. Am J Sports Med 2010;38:880–890.
Mankin HJ, Dorfman H, Lippiello L, Zarins A. Biochemical and metabolic abnormalities in articular cartilage from osteo-arthritic human hips: II. Correlation of morphology with biochemical and metabolic data. J Bone Joint Surg Am 1971;53:523–537.
Nam K, Rosado-Mendez IM, Wirtzfeld LA, Kumar V, Madsen EL, Ghoshal G, Pawlicki AD, Oelze ML, Lavarello RJ, Bigelow TA, Zagzebski JA, O'Brien WD Jr, Hall TJ. Cross-imaging system comparison of backscatter coefficient estimates from a tissue-mimicking material. J Acoust Soc Am 2012;132:1319–1324.
Nieminen HJ, Saarakkala S, Laasanen MS, Hirvonen J, Jurvelin JS, Toyras J. Ultrasound attenuation in normal and spontaneously degenerated articular cartilage. Ultrasound Med Biol 2004;30:493–500.
Nieminen HJ, Toyras J, Rieppo J, Nieminen MT, Hirvonen J, Korhonen R, Jurvelin JS. Real-time ultrasound analysis of articular cartilage degradation in vitro. Ultrasound Med Biol 2002;28:519–525.
Nieminen HJ, Zheng YP, Saarakkala S, Wang Q, Toyras J, Huang YP, Jurvelin JS. Quantitative assessment of articular cartilage using high-frequency ultrasound: Research findings and diagnostic prospects. Crit Rev Biomed Eng 2009;37:461–494.
Oelze ML, O'Brien WD. Defining optimal axial and lateral resolution for estimating scatterer properties from volumes using ultrasound backscatter. J Acoust Soc Am 2004;115:3226–3234.
Oelze ML, O'Brien WD. Application of three scattering models to characterization of solid tumors in mice. Ultrason Imaging 2006;28:83–96.
Oelze ML, O'Brien WD, Blue JP, Zachary JF. Differentation and characterization of rat mammary fibroadenomas and 4 T1 mouse carcinomas using quantitative ultrasound imaging. IEEE Trans Med Imaging 2004;23:764–771.
Pellaumail B, Watrin A, Loeuille D, Netter P, Berger G, Laugier P, Saied A. Effect of articular cartilage proteoglycan depletion on high frequency ultrasound backscatter. Osteoarthritis Cartilage 2002;10:535–541.
Pinto D, Robertson MC, Hansen P, Abbott JH. Cost-effectiveness of nonpharmacologic, nonsurgical interventions for hip and/or knee osteoarthritis: Systematic review. Value Health 2012;15:1–12.
Poole CA. Articular cartilage chondrons: form, function and failure. J Anat 1997;191(Pt 1):1–13.
Pritzker KP, Gay S, Jimenez SA, Ostergaard K, Pelletier JP, Revell PA, Salter D, van den Berg WB. Osteoarthritis cartilage histopathology: Grading and staging. Osteoarthritis Cartilage 2006;14:13–29.
Saarakkala S, Laasanen MS, Jurvelin JS, Toyras J. Quantitative ultrasound imaging detects degenerative changes in articular cartilage surface and subchondral bone. Phys Med Biol 2006;51:5333–5346.
Saarakkala S, Toyras J, Hirvonen J, Laasanen MS, Lappalainen R, Jurvelin JS. Ultrasonic quantitation of superficial degradation of articular cartilage. Ultrasound Med Biol 2004;30:783–792.
Saarakkala S, Wang SZ, Huang YP, Jurvelin JS, Zheng YP. Characterization of center frequency and bandwidth of broadband ultrasound reflected by the articular cartilage to subchondral bone interface. Ultrasound Med Biol 2011;37:112–121.
Schöne M, Männicke N, Gottwald M, Göbel F, Raum K. 3-D high-frequency ultrasound improves the estimation of surface properties in degenerated cartilage. Ultrasound Med Biol 2013;39:834–844.
Schöne M, Raum K. Inclination dependence of acoustical surface parameters obtained by ultrasound biomicroscopy for improved cartilage characterization. Biomed Tech 2011;55:138–141.
Tunis AS, Czarnota GJ, Giles A, Sherar MD, Hunt JW, Kolios MC. Monitoring structural changes in cells with high-frequency ultrasound signal statistics. Ultrasound Med Biol 2005;31:1041–1049.
Van der Sluijs JA, Geesink RG, van der Linden AJ, Bulstra SK, Kuyer R, Drukker J. The reliability of the Mankin score for osteoarthritis. J Orthop Res 1992;10:58–61.
Viren T, Saarakkala S, Jurvelin JS, Pulkkinen HJ, Tiitu V, Valonen P, Kiviranta I, Lammi MJ, Toyras J. Quantitative evaluation of spontaneously and surgically repaired rabbit articular cartilage using intra-articular ultrasound method in situ. Ultrasound Med Biol 2010;36:833–839.
Viren T, Saarakkala S, Tiitu V, Puhakka J, Kiviranta I, Jurvelin J, Toyras J. Ultrasound evaluation of mechanical injury of bovine knee articular cartilage under arthroscopic control. IEEE Trans Ultrason Ferroelectr Freq Control 2011;58:148–155.
Viren T, Timonen M, Tyrvainen H, Tiitu V, Jurvelin JS, Toyras J. Ultrasonic evaluation of acute impact injury of articular cartilage in vitro. Osteoarthritis Cartilage 2012;20:719–726.
Wang SZ, Huang YP, Saarakkala S, Zheng YP. Quantitative assessment of articular cartilage with morphologic, acoustic and mechanical properties obtained using high-frequency ultrasound. Ultrasound Med Biol 2010;36:512–527.
Yang KGA, Saris DBF, Dhert WJA, Verbout AJ. Osteoarthritis of the knee: current treatment options and future directions. Current Orthopaedics 2004;18:311–320.

APPENDIX 1

The 14-point modified Mankin score (Mankin et al. 1971; van der Sluijs et al. 1992) comprises the following categories: surface structure, cellular abnormalities, matrix staining and tidemark integrity. This study refers to surface structure as Mankin I and to cellular abnormalities as Mankin II. Table 3 provides an overview of the scoring criteria.

APPENDIX 2

The planar PMMA reflector and agar-graphite phantom were scanned in B(z) mode, that is, successive B-scans with varying transducer-sample distance. Spectra were calculated by fast Fourier transform from time gated-signals (gate type: Hanning window; gate length: 150 ns), which were located around the surface reflection for the planar reflector and 60 ns below the surface for the agar-graphite

Table 3. Scoring criteria for the used subset of the 14-point Mankin score: Mankin I and Mankin II

Structure: Mankin I	
0	Normal
1	Irregular surface, including fissures into the radial layer
2	Pannus
3	Superficial cartilage layers (≥6) absent
4	Slight disorganization (cellular rows absent, some small superficial clusters)
5	Fissures into calcified cartilage layer
6	Disorganization (chaotic structure, clusters, osteoclast activity)
Cellular abnormalities: Mankin II	
0	Normal
1	Hyper-cellularity, including small superficial clusters
2	Clusters
3	Hypo-cellularity

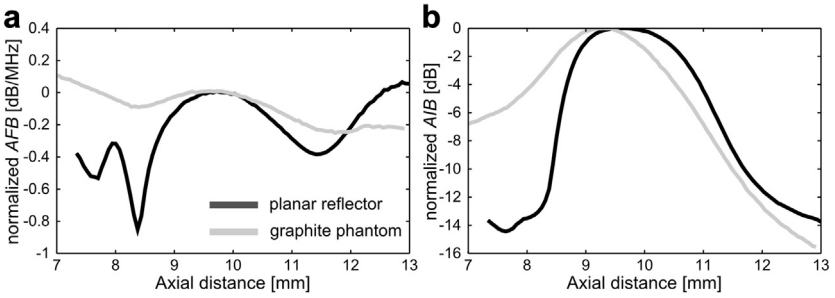

Fig. 8. Normalized spectral slope *AFB* (a) and normalized integrated spectral intensity *AIB* (b) for planar PMMA reflector and agar-graphite phantom as a function of transducer-sample distance. Because of interference artifacts of a planar reflection, a reduction in the received amplitude at the near field, as well as higher variation in the spectral slope, can be observed in comparison with a scattering target.

phantom. *AFB* and *AIB* were normalized to 0 dB/MHz at the focus position and 0 dB, respectively. The spectral slope (Fig. 8a) derived from the agar-graphite phantom exhibits a linear decrease with increasing axial distance, which can be explained by the acoustic attenuation in water as well as a deviation around the focus that can be the result of diffraction effects. By contrast, also within the focal region (–6-dB range), the spectra obtained from planar reflections were subject to much higher deviations and exhibited a large decrease in amplitude (Fig. 8b) and spectral slope at the near field of the transducer. Therefore, use of time-of-flight matched spectra obtained from a planar reflector as a reference would cause overestimation of spectral slopes at defocused time gates and was therefore avoided.